Neural Network-Based Estimation of Rebar Deflection for Robotic Rebar Installation of Vertical Structures

Hongjie Cai[1,2], Rongbo Hu[2], Ser Tong Quek[1], Soungho Chae[2], and Justin K.W. Yeoh[1]

[1]Dept. of Civil and Environmental Engineering, National University of Singapore, Singapore
[2]Kajima Technical Research Institute Singapore, Kajima Corp, Singapore

h.cai@u.nus.edu , r.hu@kajima.com.sg, ceeqst@nus.edu.sg, s.chae@kajima.com.sg, justinyeoh@nus.edu.sg

Abstract -
In construction, most existing research on rebar placement focuses on guardrail system for large-scale planar slabs or multi robot arm system for off-site rebar cage assembly, frequently utilizing gantry systems. However, their substantial setup time and spatial requirements greatly reduce their suitability for smaller-scale or more spatially constrained settings. This limitation is particularly pronounced in on-site application where the rebar installation of vertical structural elements occurs in fragmented and restricted workspaces, limiting the applicability of existing guardrails or multiple robotic systems. To address this gap, this study investigates the feasibility of employing a single arm robotic system to grasp and position rebar for vertical structural components. One critical challenge in this context is to account for rebar deflection during rebar placement operations. Moreover, existing analytical equations do not provide sufficiently accurate deflection estimates. To address this problem, a neural network model was developed to predict rebar deflection across a range of sizes and lengths, allowing the robot to adapt its position dynamically according to the target location. The proposed model achieved an R^2 accuracy of 0.9714 and outperformed other models in both the ±0.01m and ±0.092m thresholds, demonstrating its effectiveness in providing precise deflection estimates. This level of precision facilitates efficient robotic rebar placement using a single-arm system.

Keywords -

Construction robotics; Rebar Installation; Rebar Deflection; Neural Networks

1 Introduction

The construction industry has long been recognized as a labor intensive and inherently hazardous field, characterized by physically demanding tasks, challenging work environments, and a high risk of injuries [1]. Over the years, researchers and innovators have directed significant efforts toward addressing these challenges through the development and deployment of construction robots. Such technologies promise to mitigate labor shortages, enhance workplace safety, and boost operational efficiency.

However, despite these advancements, the widespread integration of construction robots remains limited, particularly in structural work, an essential component often found on the project's critical path. Reinforcement bar (rebar) placement, specifically, is a crucial structural activity directly influencing the structural integrity, durability, and safety of reinforced concrete structures. Manual rebar placement can be labor-intensive, prone to errors, and subject to variable quality. Automating rebar placement presents significant opportunities for improving industry-wide efficiency, precision, and safety, marking it as a high-priority area for innovation.

Most existing research has focused on horizontal structures such as planar slabs and precast panels, while vertical structures have received far less attention. Yet vertical components which are on-off or low-repetition require in-situ casting, such as soil-retaining walls and water tanks that common in housing and infrastructure project. For infrastructure projects in particular, most of vertical elements are also cast in situ, because most of them are designed as one-off components. Moreover, Many existing robotic solutions for rebar placement are complex and space-intensive (e.g. gantry with multi-arm), requiring extensive setup and wide, unobstructed work areas that typical construction sites cannot provide. To address these shortcomings, this study investigates the feasibility of a single-arm robotic system for rebar placement in vertical structures.

In horizontal assemblies, rebar deflection is limited to the lifting phase and is naturally resolved upon placement. However, for vertical structures, deflection remains a critical factor that must be addressed throughout the placement process. Existing research primarily focuses on deflection in reinforced concrete or steel beams, with no attention given to the deflection behavior of standalone rebars. Furthermore, existing formulas are inadequate for accurately predicting rebar deflection due to the irregular shape of rebar. Therefore, the primary objective of this study is to identify an effective method to estimate deflection under cantilever conditions, providing a foundation for single-arm robotic rebar placement in vertical structural components.

2 Literature Review

2.1 Robotic or automation for rebar placement

Some rebar palcement system have been explored and developed over the past few decades, for example the IronBot [2] was used for bridge deck rebar installation and the multi-manipulator gantry system described by Mahdi Momeni et al. [3] for prefabricated rebar cages, are effective in controlled factory or open-site environments. However, their extensive setup time, large footprint, and need for clear working envelopes limit their practicality on most housing and many infrastructure projects, where sites are fragmented and space constrained

Additionally, Zhang et al. [4] use a off-the-shelf kuka robot arm for tasks like rebar picking, transportation, and placement. However, the study used short rebars for demonstration, allowing deflection to be ignored, and was limited to planar mesh construction. Dörfler et al.[5] presented the Mesh Mould system, an innovative mobile robotic setup capable of fabricating vertical freeform structural wall on site. However, the system relied on short steel wire segments rather than the long rebars conventionally employed in typical construction practices.

In summary, existing automated rebar placement systems primarily focus on planar slab construction, often using short rebars that do not account for deflection. Currently, no research explores the use of a single-arm robotic system for long rebar placement in vertical structures.

2.2 Estimation of deflection of beam

The Euler–Bernoulli beam theory is a fundamental method for analyzing beam deflection. It assumes linear elastic behavior, small deflections, and negligible shear deformation, making it suitable for long, slender beams under relatively small loads [6]. The relationship between bending moment and curvature is expressed in Equation 1:

$$M = EI\frac{d^2w}{dx^2} \tag{1}$$

where M is the bending moment, E is Young's modulus, I is the moment of inertia, and w is the deflection.

Elementary beam theory neglects the square of the first derivative in the curvature formula, making it unsuitable for scenarios involving large deflections. In contrast, large deflection theory considers both initial and deformed configurations of the beam axis [7], capturing phenomena like significant rotational effects in flexible structures. Due to the mathematical complexity of these nonlinear equations, analytical solutions are often impractical, and numerical methods—such as Finite Element Analysis (FEA) tools like ANSYS and ABAQUS—are widely used. For instance, Yuan et al. [8] applied numerical methods to analyze steel beams with octagon-web designs, achieving improved accuracy in deflection predictions.

While beam deflection theories are well-studied in structural engineering, most research focuses on composite structures like reinforced concrete or steel beams with larger moments of inertia. However, there is a notable lack of investigation into the deflection behavior of rebar as an individual structural element. This gap highlights the need for focused research in this area.

3 Methods

3.1 One-arm robot for rebar placement

In this study, a single robotic arm is used for rebar placement, with an RGB-D camera detecting the position and intersection of the rebar. Figure 1 shows two cases of rebar gripping and placement: in the top diagram, the robotic gripper holds the rebar at its center, causing the ends to bend downward; in the bottom diagram, the gripper holds the rebar at one end, allowing the opposite end to deflect freely. The dashed red line indicates the target position, and the solid green line represents the actual deformation when gripped.

The workflow is outlined in Figure 2. After receiving the rebar's target size and location, the robot retrieves the rebar and moves it to the intended position. Using vision-based detection, the system calculates the error between the actual and target positions. If the error exceeds 10 mm, feedback is sent to adjust the rebar's position until it falls within the fluorescence zone, ensuring accurate placement.

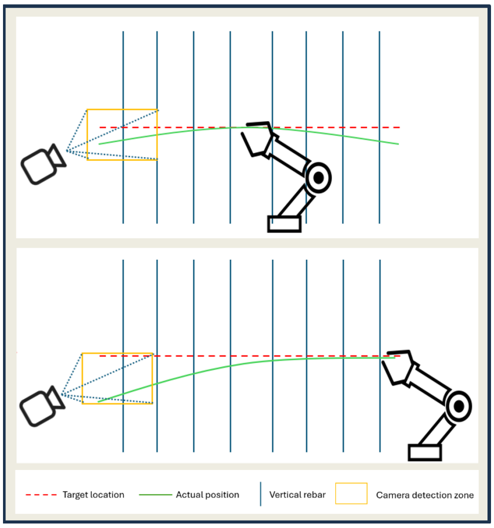

Figure 1. Two scenarios of one robot arm rebar placement system

Accurate deflection estimation is crucial for two reasons: 1) keeping the intersection point within the camera's detection range ensures proper operation, and 2) improved estimation increases the likelihood of errors being within the 10 mm threshold, reducing repositioning.

The Intel RealSense D435 camera, with a horizontal FOV of 69° and vertical FOV of 42° is used [9]. The detection zone can be calculated using Equation 2 [10]:

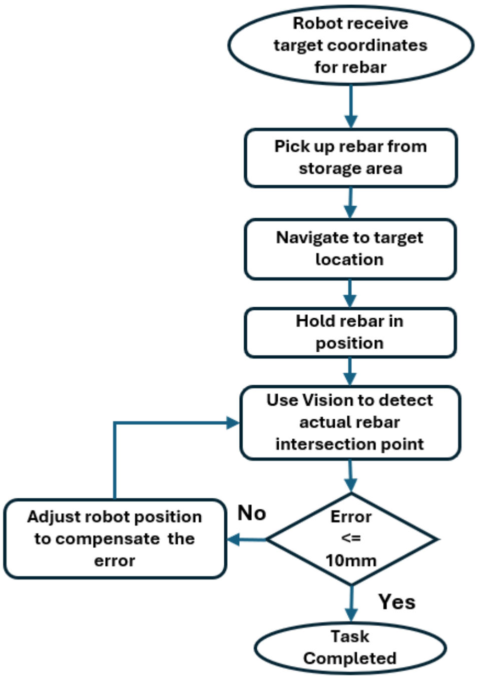

Figure 2. Flow chart for rebar placement

$$\text{Dimension} = 2 \times \text{Distance} \times \tan\left(\frac{\text{FOV}}{2}\right) \tag{2}$$

Where dimension is either Width (using Horizontal FOV) or Height (using Vertical FOV).

For example, as shown in Figure 3, positioning the camera 0.30 m from the target yields a viewing window of roughly 0.41 m × 0.23 m. After restricting analysis to the central 80 % region of interest (ROI)[9], permitting detection of deflections up to about 0.092 m below the target binding point; larger sag will lie outside this effective window. Moving the camera farther back can enlarge the coverage area but at the cost of potential loss of image fidelity [11].

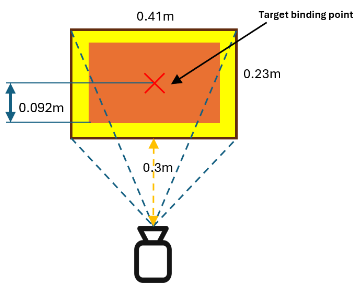

Figure 3. Illustration of camera detection zone

While no specific tolerance for rebar spacing is stated in Eurocode or Singapore Standards, common practice in Singapore allows a tolerance of ±10mm from the designed spacing. In the United States, according to ACI 117-10 [12], the tolerance for wall thicknesses between 4 to 12 inches is ±3/8 inch (approximately 10mm). Thus, ensuring the rebar deflection estimation remains within 10mm of the target location could significantly minimize the need for repeated repositioning of the robot gripper and improve operational efficiency.

3.2 Estimation of rebar deflection

In this study, four different models were developed to predict deflection behavior: two theoretical models—the Euler-Bernoulli equation and large deflection theorem conducted in ANSYS, and two data-driven models—a nonlinear regression model and a neural network model—built using empirical data from experimental testing.

Model accuracy was judged by the coefficient of determination (R^2), which measures the proportion of variance in the dependent variable explained by the independent variables, and the mean absolute error (MAE), the average magnitude of prediction errors. Additionally, two threshold - ±0.092 (camera detetction zone) and ±0.01 m (construction tolerance) were also applied to verify the performance of the predictions stayed within practical limits.

For the purposes of this study, it was assumed that the rebar is firmly grasped by the robotic gripper, simulating a cantilever boundary condition. The estimation process utilized two input variables: the length and diameter of the rebar, with the output being the deflection of the rebar. Common material properties were applied across all techniques, including an elasticity modulus of 200 GPa, a density of 7850kg/m3, and a gravitational acceleration of 9.81m/s2.

3.2.1 Theoretical and numerical estimation

Initial deflection estimations were conducted using two primary approaches: the Euler–Bernoulli beam theory and the finite element method (FEM) performed in ANSYS. The Euler–Bernoulli beam theory was first employed, providing a theoretical framework based on assumptions of linear elasticity and small deflection behavior. The maximum deflection $\delta_{\max}$ under self-weight was calculated using the equation 3:

$$\delta_{\max} = \frac{\omega L^4}{8EI} \tag{3}$$

where ω is the distributed load, L is the length of the rebar, E is the modulus of elasticity, I is the moment of inertia.

To address potential geometric non-linearity, the large deflection theorem was applied. This approach considers large displacements and provides more accurate predictions for long rebars. The large deflection analysis were performed using ANSYS to supplement the theoretical models and provide a computational perspective on deflection behavior (Figure 4).

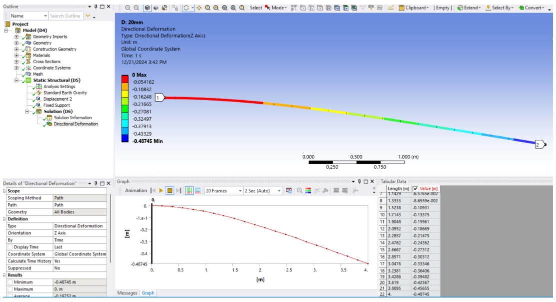

Figure 4. ANSYS analysis of rebar deflection

3.2.2 Experimental data collection

To validate the theoretical predictions and provide data for subsequent nonlinear regression analysis and neural network training, an experimental study was conducted. Rebars of varying lengths and diameters were tested under self-weight in a cantilever setup, where one end was securely fixed to a workbench using two clamps, and the other end was left free to deflect, as illustrated in Figures 5. Deflections at the free end were measured using laser displacement sensors (Leica DISTOTM X4).

Figure 5. Rebar deflection experiment set up

The experiment involved a total of 27 rebars, with diameters ranging from 10mm to 32mm and lengths ranging from 2.5m to 4m. Each rebar was tested multiple times (4-6 trials) at different cantilever lengths, resulting in a total of 154 data points. These measurements served as the foundation for evaluating the accuracy of the theoretical models and for developing data-driven predictive methods.

3.2.3 Training of Nonlinear Regression Model

To predict rebar deflection, a nonlinear regression model was developed using experimental data. The relationship between the key inputs—rebar length (L) and diameter (d) of the rebar—and the deflection $\delta_{\max}$ was modelled using the "`curve_fit`" function from Python's SciPy library. This regression analysis aimed to find the best-fit equation by minimizing the residual error between the predicted and observed values, producing a model that accurately reflects real-world behavior. The dataset was randomly split into 70% for training and 15% for testing using the "`train_test_split`" function from Python's scikit-learn library. The training set and testing set are the same for both nonlinear regression model and neural network model. The remaining 15% is validation set, which is only used in neural network model training.

The equation for maximum deflection is expressed in the general form:

$$\delta_{max} = aL^b d^c \tag{4}$$

where a, b, and c are coefficients of the regression.

Considering the mechanics of deflection, it is influenced by the rebar's self-weight (proportional to its density) and length, while being inversely proportional to material stiffness and cross-sectional properties. Incorporating these relationships, the equation is refined as:

$$\delta_{\max} = e\frac{\rho g L^f}{E d^h} \tag{5}$$

Where ρ is density of the material, g is the gravitational acceleration, E is the modulus of the elasticity. and e, f, and h are coefficients to be determined through regression.

This refined equation links deflection to fundamental physical parameters, ensuring the model aligns with theoretical expectations. By determining the values of e, f, and h through regression analysis, providing a practical equation for estimating rebar deflection under self-weight.

3.2.4 Training of Neural Network Model

The predictive model for estimating deflection employs a neural network architecture designed to capture the relationship between two primary input features: Diameter and Length. As shown in Figure 6, the network consists of a single hidden layer with 256 neurons, utilizing the ReLU activation function to learn complex, non-linear relationships. The final output layer contains a single neuron without an activation function, suitable for regression tasks.

The hyper-parameter tuning process was conducted to optimize the neural network architecture for deflection prediction. Various configurations were evaluated, including single-layer and multi-layer architectures, with a single hidden layer selected for its simplicity and performance. The number of neurons was varied from 64 to 512, with 256 neurons chosen as the optimal configuration. Regularization methods such as L2 regularization (0.01 to 0.0001) and dropout (0.01 to 0.5) were tested but excluded in the final model as they did not improve performance. The Adam optimizer and mean squared error (MSE) loss function ensured efficient convergence.

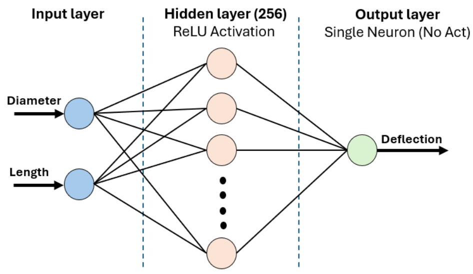

Figure 6. Neural Network Architecture

4 Results

4.1 Results of different models

The graph in Figure 7 illustrates the deflection of seven different rebar diameters under self-weight in a cantilever boundary condition, as predicted by the Euler–Bernoulli equation, FEA (large deflection), non-linear regression model, neural network model, and the actual experimental measurements. For the non-linear regression and neural network models, data from only the first trial run are presented in the graph. Trend lines are included for each model to improve visualization and facilitate a clearer comparison of accuracy among the four predictive models.

In addition, comprehensive evaluations were conducted across various diameters and length ranges using all available data points. Metrics including R^2, MAE, and the percentages of predictions falling within two accuracy thresholds (±0.092 m and ±0.01 m) were computed for each method—the Euler-Bernoulli equation, the non-linear regression model, and the neural network model. These results are summarized in Tables 1 and 2, with the best-performing method in each category highlighted in bold. However, the FEA was excluded from this detailed analysis due to the significant computational time required to run simulations. Running simulations for all 154 combinations of diameters and lengths to calculate comparable values was deemed impractical.

For both the non-linear regression and neural network models, training, validation, and testing datasets were randomly assigned. To ensure robustness, additional five trial runs were conducted for each model, using identical datasets across both models in each run. This approach also helps to verify that if the result in Table 1 was representative of the overall models' performance. The data presented here is derived from the testing dataset, providing a more reliable basis for comparison between the non-linear regression and neural network models. A detailed summary of these results is provided in Table 3.

4.2 Regression equation of non-linear model

To develop the regression model, parameters e, f, and h were estimated for each trial, and the ressult were listed on Table 4. These parameters define the model's ability to relate the input variables to the target output. The average values of these parameters were used to construct the regression equation, which is expressed as Equation 6.

$$\delta_{\max} = 10\frac{\rho g L^{3.61}}{E d^{1.75}} \tag{6}$$

4.3 Model fitting of neural network

Figure 8 shows the training and validation loss curves, which are closely aligned, indicating that the model generalizes well to unseen data. Both loss curves drop sharply

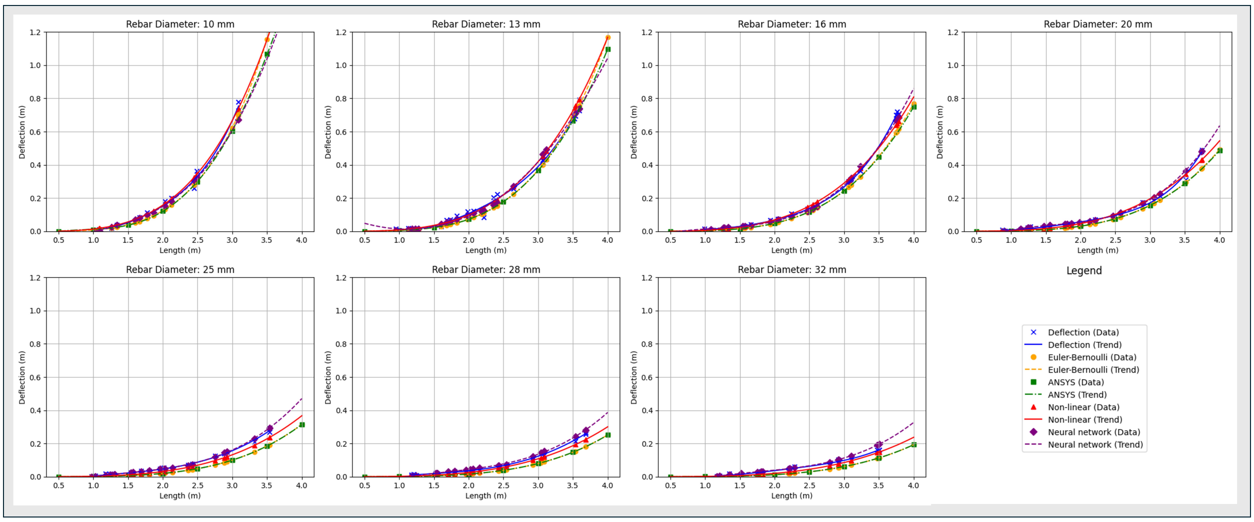

Figure 7. Trend-line comparison between measured deflection and predictions from four estimation methods

Table 1. Comparison among different models for different diameters.

Diameter (mm)	R^2			MAE (m)			±0.01 m(%)			±0.092 m(%)		
	Euler-Bernoulli	Non-linear	Neural-network	Euler-Bernoulli	Non-linear	Neural-network	Euler-Bernoulli	Non-linear	Neural-network	Euler-Bernoulli	Non-linear	Neural-network
10	0.9779	**0.9895**	0.9805	0.0252	**0.0164**	0.0208	31.25	**56.25**	**56.25**	93.75	**100**	93.75
13	0.9843	0.9850	**0.9874**	0.0264	0.0238	**0.0231**	21.74	**26.09**	**26.09**	**100**	**100**	**100**
16	0.9647	0.9911	**0.9966**	0.0294	0.0147	**0.0099**	18.18	63.64	**68.18**	86.36	**100**	**100**
20	0.9285	0.9810	**0.9834**	0.0261	0.0142	**0.0124**	18.18	**54.55**	45.45	90.91	**100**	**100**
25	0.7630	0.9417	**0.9894**	0.0318	0.0168	**0.0066**	13.64	22.73	**77.27**	90.91	**100**	**100**
28	0.7847	**0.9629**	0.9613	0.0289	0.0130	**0.0125**	9.09	40.91	**45.45**	**100**	**100**	**100**
32	0.6772	**0.9341**	0.8789	0.0260	**0.0113**	0.0135	22.22	50.00	**61.11**	93.26	**100**	**100**

Table 2. Comparison among different models for different lengths.

Length (m)	R^2			MAE (m)			±0.01 m(%)			±0.092 m(%)		
	Euler-Bernoulli	Non-linear	Neural-network	Euler-Bernoulli	Non-linear	Neural-network	Euler-Bernoulli	Non-linear	Neural-network	Euler-Bernoulli	Non-linear	Neural-network
0.5m-1.5m	-0.3522	0.1260	**0.4395**	0.0082	0.0065	**0.0052**	54.05	75.68	**83.78**	**100**	**100**	**100**
1.5m-2m	0.3510	0.7459	**0.8991**	0.0202	0.0128	**0.0071**	15.15	39.39	**75.76**	**100**	**100**	**100**
2m-2.5m	0.8045	0.9225	**0.9304**	0.0308	0.0166	**0.0142**	0.00	40.00	**50.00**	**100**	**100**	**100**
2.5m-3m	0.3228	0.8406	**0.9673**	0.0354	0.0162	**0.0070**	7.69	30.77	**84.62**	**100**	**100**	**100**
3m-3.5m	0.9597	**0.9852**	0.9572	0.0353	**0.0195**	0.0330	6.67	**26.67**	13.33	93.33	**100**	93.33
3.5m-4m	0.8884	0.9644	**0.9833**	0.0678	0.0379	**0.0251**	0.00	**17.65**	**17.65**	47.07	**100**	**100**

Table 3. Five trial run results of non-linear and neural-network models.

Trial Run	TestingR^2		Testing MAE (m)		±0.01 m (%)		±0.092 m (%)	
	Non-linear	Neural network	Non-linear	Neural network	Non-linear	Neural network	Non-linear	Neural network
1	0.9434	**0.9739**	0.0158	**0.0119**	33.33	**66.67**	**100**	**100**
2	**0.9675**	0.9638	0.0196	**0.0168**	20.83	**58.33**	**100**	**100**
3	0.9784	**0.9943**	0.0154	**0.0082**	33.33	**62.50**	**100**	**100**
4	0.9812	**0.9815**	0.0248	**0.0195**	25.00	**41.67**	95.83	**95.83**
5	**0.9789**	0.9433	0.0168	**0.0138**	29.17	**41.67**	95.83	**100**
Average	0.96988	**0.97136**	0.01848	**0.01404**	28.33	**54.17**	98.33	**99.17**

Table 4. Values of non-linear regression parameters

	e	f	h
1	10.0	3.6779	1.7355
2	10.0	3.5625	1.7632
3	10.0	3.6695	1.7386
4	10.0	3.6038	1.7548
5	10.0	3.5535	1.7692
Average	10.0	3.61344	1.75226

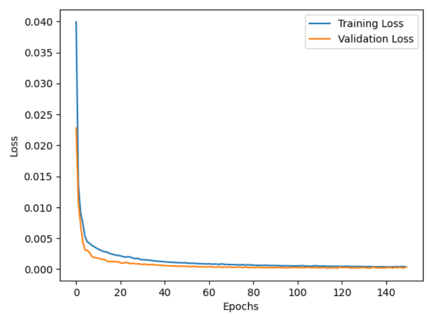

Figure 8. training vs validation loss

in the initial epochs and subsequently plateau, demonstrating that the network has effectively learned the underlying data patterns without exhibiting signs of overfitting or underfitting.

5 Discussion

5.1 Analysis and comparison of model results

Figure 7 shows that both the Euler–Bernoulli and large deflection models closely match the actual deflection values for shorter rebar lengths. However, as the rebar length increases, these models increasingly underestimate deflections, resulting in conservative predictions.

In contrast, the non-linear regression and neural-network models both sustain high predictive quality over the full span of rebar diameters and lengths: their trendlines track the measured deflections closely, confirming their superior accuracy and robustness in modelling deflection behaviour for a wide range of geometries.

Detailed numerical comparisons are presented in Tables 1 and 2. Both the neural network and non-linear regression models generally achieved higher R^2 values than the Euler–Bernoulli equation across every diameters and lengths. Diameter-wise, the non-linear regression model has a slight edge over the neural network for several sizes, whereas length-wise the neural network leads in all categories except the 3–3.5 m interval.

In terms of MAE, the neural network consistently produced the lowest values across both diameter and length ranges, , except for the 3-3.5 m, indicating its superior absolute accuracy. The non-linear regression model also consistently performed better than the Euler–Bernoulli equation, highlighting the inherent limitations of linear-elastic assumptions for predicting complex deflection behaviors.

Most importantly, when evaluating performance based on practical accuracy thresholds (±0.01 m and ±0.092 m)—a key focus of this study—the neural network and non-linear regression models clearly outperformed the Euler–Bernoulli equation. Under the stringent ±0.01 m criterion, the neural network delivers the highest within-tolerance rate for almost all lengths and diameters. With the more lenient ±0.092 m threshold, both data-driven models achieve near-perfect accuracy, far surpassing Euler–Bernoulli—particularly for the longer bars.

A notable discrepancy is observed for parameters of 10 mm diameter and 3–3.5 m length, where the neural network model underperforms relative to the nonlinear regression model, despite its otherwise comparable or superior performance. This exception is likely a training-specific artefact: the particular network realisation appears to have missed one or two points in that band. To test whether this weakness is systematic, we retrained both models five times on identical, randomly drawn training–testing splits and compared with non-linear regression model with same testing set in each run.

As Table 3 shows, across the five runs, each model sustained an average testing R^2 values of approximately 0.97. The neural network further lowered the MAE by about 4.5 mm relative to the non-linear regression. For the broader ±0.092 m threshold, both models achieved similarly high accuracy, with the neural network slightly ahead (99.17%) compared to the non-linear regression model (98.33%). However, for the stricter ±0.01 m threshold, the neural network significantly outperformed the non-linear regression model, achieving nearly double the percentage of accurate predictions (54.17% vs. 28.33%). This substantial difference highlights the neural network model's greater capability in capturing subtle variations in rebar deflection, and the earlier 3–3.5 m anomaly is a model-realisation outlier rather than an inherent limitation.

In summary, both the non-linear regression and neural network models demonstrate superior robustness in predicting rebar deflection and consistently outperform the numerical models in all metrics. However, the neural network model excels in fine-grained precision, making it the most effective approach for accurate rebar deflection estimation.

5.2 Factors influencing rebar deflection

One possible explanation for the increased deflection is the fact that rebar is not perfectly round. The rebar used in the test complies with the BS4449:2005 standard (Grade: B500B) and features transverse and longitudinal ribs on its surface, which are designed to enhance the bonding between the concrete and the rebar [13]. However, these ribs are not accounted for in the estimated mass or cross-sectional area when using the nominal diameter, as the actual core diameter is slightly smaller than the nominal diameter. This discrepancy is illustrated in Figure 9 [14]. The irregular shape is likely a primary factor contributing to the larger deflection observed compared to theoretical predictions based on simulations or calculations assuming a regular, perfectly round steel bar. The irregularities in the shape lead to a non-uniform distribution of material. The effective moment of inertia will likely be lower than that of the nominal circular shape due to the reduced symmetry and possible loss of material at certain points.

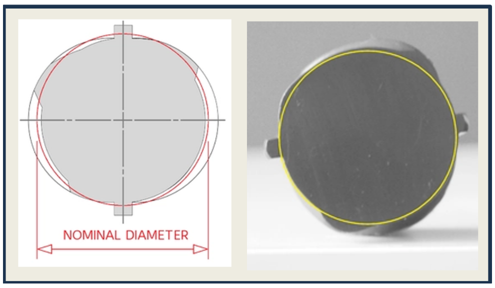

Figure 9. Actual cross section of rebar

Additionally, Orientation or gripping point may also influence deflection, but consistent orientation is impractical on site, so bars were randomly oriented for testing. The measured deflection data, presented in Figure 7, were obtained from rebars of varying sizes and orientations. Although some variation exists, the data points consistently follow a similar trend, indicating that orientation is not a critical factor influencing deflection.

In conclusion, irregularities in rebar geometry pose significantly challenges for accurate prediction of deflection using numerical models, as indicated by the consistently large MAE observed across different rebar sizes. These results underscore the necessity for developing more advanced predictive models that effectively account for geometric irregularities.

5.3 Impact to the robot rebar palcement

With the improved accuracy in rebar deflection estimation, the use of a single robotic arm for rebar placement becomes a viable solution. The higher prediction accuracy increases the likelihood of maintaining deflection within the required tolerance, minimizing the need for repeated intersection detection and position adjustments. This enhancement streamlines construction workflows, improving both efficiency and precision.

Additionally, accurate prediction of rebar deflection plays a critical role in other stages of rebar handling. For example, the motion planning of the robotic arm must consider predicted deflection to avoid collisions with objects during movement. Deflection estimation is also essential when determining the optimal gripping points, ensuring effective handling of the rebar.

6 Conclusion

This study emphasizes that managing rebar deflection during placement is a significant challenge when utilizing single robotic arm systems for rebar placement in vertical structural elements.

It also underscores the limitations of existing theoretical models, which fail to accurately predict standalone rebar deflection under real-world conditions. By integrating experimental data, the development of a neural network model effectively addresses these gaps, achieving nearly 100% likehood of fall within the camera's field of view and over a 50% likelihood of placing the rebar within 10mm of the target location. This advancement provides a more reliable and practical predictive tool for robotic rebar placement applications.

However, certain limitations should be acknowledged. For instance, further research is necessary to comprehensively identify and evaluate factors that lead to larger deflections, including rebar geometry and environmental influences such as corrosion and temperature variations. Moreover, this study is limited to the initial rebar intersection placement, leaving the complexities associated with subsequent intersections unaddressed. Exploring these challenges represents a valuable direction for future work.

References

[1] Pei Pei Heng, Hanizah Mohd Yusoff, and Rozita Hod. Individual evaluation of fatigue at work to enhance the safety performance in the construction industry: A systematic review. *PLoS one*, 19(2):e0287892, 2024.

[2] IronBOT | rebar lifting, carrying, and self-placing robot. URL `https://www.constructionrobots.com/ironbot`.

[3] Mahdi Momeni, Johan Relefors, Abubakar Khatry, Lars Pettersson, Alessandro V Papadopoulos, and Thomas Nolte. Automated fabrication of reinforcement cages using a robotized production cell. *Automation in Construction*, 133:103990, 2022.

[4] Jiansong Zhang, Chen Shen, and Ruilin Li. A robotic system method and rebar construction with off-the-shelf robots. In *Computing in Civil Engineering 2021*, pages 1204–1211. 2021.

[5] Kathrin Dörfler, Norman Hack, Timothy Sandy, Markus Giftthaler, Manuel Lussi, Alexander N Walzer, Jonas Buchli, Fabio Gramazio, and Matthias Kohler. Mobile robotic fabrication beyond factory conditions: Case study mesh mould wall of the dfab house. *Construction robotics*, 3:53–67, 2019.

[6] Oliver A Bauchau and James I Craig. Euler-bernoulli beam theory. In *Structural analysis*, pages 173–221. Springer, 2009.

[7] KE Bisshopp and DC13360 Drucker. Large deflection of cantilever beams. *Quarterly of applied mathematics*, 3(3):272–275, 1945.

[8] Ling Yuan, Bi Sun, Lu Ma, Weidong Wu, et al. Research on factors affecting deflection and an approach for evaluating web stress for steel octagon-web beam. *Heliyon*, 9(7), 2023.

[9] Intel realsense camera 400 series product family datasheet. Datasheet 337029-017, Intel Corporation, March 2024. URL `https://www.intelrealsense.com/wp-content/uploads/2024/10/Intel-RealSense-D400-Series-Datasheet-October-2024.pdf`. Revision 018.

[10] Richard Szeliski. *Computer vision: algorithms and applications*. Springer Nature, 2022.

[11] Chanda Bhabatosh et al. *Digital image processing and analysis*. PHI Learning Pvt. Ltd., 2011.

[12] American Concrete Institute. *Specification for Tolerances for Concrete Construction and Materials (ACI 117-10) and Commentary*. American Concrete Institute, Farmington Hills, MI, 2010.

[13] BSI BS 4449. Steel for the reinforcement of concrete—weldable reinforcing steel—bars, coil and decoiled product—specification. *Standard Policy and Strategy Committee*, pages 1–27, 2005.

[14] Betonstaal. Rebar isn't round at all, n.d. URL `https://www.betonstaal.nl/en/knowledge-centre/rebar-isnt-round-at-all`. Accessed: 2025-01-02.